Anharmonicity of quantum meta-atoms due to dynamic anapole state

I. Stenishchev,[1] S. Gilmulin,[1] G. Matveev,[1] N. S. Smirnov,[2] D. O. Moskalev,[2] A. A. Pishchimova,[2] I. A. Rodionov,[2,*] and A. A. Basharin[1,†]

[1]*Department of the Theoretical Physics and Quantum Technologies, National University of Science and Technology MISIS, 119049 Moscow, Russia*

[2]*FMN Laboratory, Bauman Moscow State Technical University, 105005 Moscow, Russia*

(Received 17 October 2023; revised 29 June 2024; accepted 9 July 2024; published 25 July 2024)

Anapole electrodynamics is now a rapidly developing area of nonradiating and invisible systems like metamaterials, nanoparticles, and even toroidal optical transitions in hydrogenlike atoms from microwaves to optics. The main advantages are demonstrated strong localized near fields and an extremely high Q factor due to the absence of radiating losses. In this paper, we expand the field of anapole electrodynamics to the quantum area and demonstrate the anharmonicity of a superconducting meta-atom with an embedded Josephson junction. The maximum dimension of meta-atoms is 6 mm, and it works in the microwave range. The microwave single- and two-tone spectroscopic measurements in a dilution cryostat at 20 mK demonstrate three transition energy levels: single-photon and two-photon transitions. Moreover, we obtain an anharmonicity of 540 kHz, which is very close to 500 kHz obtained in simulations. We show that the anapole meta-atoms are promising candidates for giant qubits for quantum computing applications.

DOI: 10.1103/PhysRevB.110.035157

I. INTRODUCTION

It is commonly believed that the quantum properties of matter can be observed only on nano- and atomic scales. However, the second quantum revolution gave rise to an unprecedented advantage for observation of quantum states of objects even at the microscale [1]. In nature, there are a few observable and well-described two-level systems like photons, spins, neutrino, etc. [2–5]. Moreover, sufficiently anharmonic multilevel systems can be designed such as spin- and ion-trap-based [6,7] and superconducting [8,9] qubits. In some sense, this allows us to find the conditional border between the quantum and classical worlds. One well-known example is quantum meta-atoms as elements of qubits. They allowed us to find a compromise between the significant qubit lifetime and a sufficiently low Rabi frequency with increasing linear size of the qubit. Here, superconducting artificial meta-atoms are one of the most promising candidates for large-scale qubits since they can reliably implement strongly interacting individual or arrays of harmonic oscillators that are microwave cavities and slightly anharmonic oscillators based on Josephson junctions (JJs) [8,9]. Anharmonicity is obviously important for the realization of quantum systems. It helps us to distinguish the relevant transitions of different energy levels in the system. The most outstanding representations of quantum meta-atoms, the transmon [10,11] and fluxonium qubits [12–14], have a large anharmonicity, as well as significant advantages in terms of coherence times, single-qubit gate fidelities, and leakage rates [15]. Accordingly, one can distinguish different quantum levels of qubits in low-temperature experiments. Actually, the dimensions of superconducting qubits do not exceed $\sim$500 μm, which is sufficiently lower than the microwave wavelength of the excited signal [16]. Indeed, the subwavelength qubits provide suppression of radiating losses; however, this significantly reduces the efficiency of the qubits. In contrast, the large-scale qubit manifestation is caused by the presence of radiating losses in cavities since its dimensions tend to the wavelength and its dipole moment is increased [17]. On the other hand, large qubits are unaffected by solid-state parasitic effects that lead to such local overheating of the superconductors, such as Abrikosov vortices. Thus, the dilemma regarding the size and radiation losses seems to be how to realize a giant and simultaneously nonradiating meta-atom demonstrating quantum features. Recently, Zagoskin *et al.* called such a system a *quiet artificial atom* [18].

One of the best examples of the nonradiating configuration in electrodynamics is the *dynamic anapole state* [19–25] based on destructive interference between electric and toroidal dipole moments exhibiting unique electromagnetic wave properties like strong field localization [26–28], invisibility [29–34], the dynamic Aharonov-Bohm effect [35], an extremely high Q factor [36], and nanolasing [37]. A dynamic toroidal dipole possesses a radiation pattern and angular momentum identical to those of the electric dipole in the far-field zone [38,39]; however, their current configurations are absolutely different in origin [35,40]. Thus, excited by an electromagnetic wave in the same volume, the toroidal and electric dipole moments in the relation $\mathbf{P} = -ik\mathbf{T}$ form a nonradiating anapole in all-dielectric and metallic particles and metamaterials [38,41,42], as well as in hydrogenlike atoms [43]. The ideal anapole source has an extremely high Q factor and can be considered a perfect open resonator [36]. Here, we note the principal difference between the dynamic anapole and the static anapole proposed by Zel'dovich [44]. In the

*Contact author: irodionov@bmstu.ru
†Contact author: alexey.basharin@gmail.com

static case with $k = 0$, the electric moment disappears, $\mathbf{P} = 0$, thus making the static anapole of Zel'dovich synonymous with the static toroidal dipole [45]. Thus, the representation of the dynamic problem, the nonradiating anapole state, can be excited by external electromagnetic excitation (a scattering problem of individual particles or metamaterials) [19,21,22] or internal excitation like in the antenna problem [45,46].

II. THE MODEL FOR AN ANAPOLE META-ATOM

We introduce a superconducting harmonic meta-atom acting as a nonradiating system with localized electric and magnetic fields at its origin and excited by an external incident wave. The nonlinear anharmonic element, the Josephson junction, is embedded in its vicinity. In a physical sense, such a configuration is similar to a transmon.

The anharmonicity of transmons in cavities is proportional to the ratio of the magnetic power to the electric power close to a JJ, i.e., $\sim 1 - \frac{W^H}{W^E}$ [47]. It follows that the meta-atom must have a large ratio of these energies. Unfortunately, the design of the transmons known to us from the literature does not fully satisfy this condition. Therefore, new approaches are needed to develop novel meta-atoms, and the anapole approach is promising for meta-atoms since this relationship is satisfied due to the special configuration of closed magnetic fields [35].

Here, we consider the Hamiltonian of the anapole meta-atom by introducing the ratio of the magnetic field energy around the JJ to the total magnetic field energy of the surrounding media:

$$\gamma \equiv \frac{W^{\Phi}_{JJ}}{W^{\Phi}_{\text{total}}}. \tag{1}$$

In this case the Hamiltonian includes two parts:

$$\hat{H}^{\Phi}_{\text{linear}} = \underbrace{\frac{E_J\hat{\phi}^2}{2}}_{\substack{\text{linear}\\ \text{part}\\ \text{of JJ}}} + \underbrace{\frac{E_J\hat{\phi}^2}{2}\left(\frac{1}{\gamma} - 1\right)}_{\substack{\text{linear part of the}\\ \text{geometric inductance}}} = \frac{\hat{\Phi}^2}{2L}, \tag{2}$$

where Φ is magnetic flux, $E_J = \frac{I_C\Phi_0}{2\pi}$ is the Josephson energy, and I_C is the critical current. Thus, we present a complete Hamiltonian of the meta-atom with a small perturbation $\hat{V}$, where the third term characterizes the electric field of the meta-atom:

$$\hat{H} = \left(\hat{H}^{\Phi}_{\text{linear}} + \hat{V}\right) + \frac{\hat{Q}^2}{2C}, \tag{3}$$

where Q is the general charge density of the meta-atom and C is the equivalent capacitance. The perturbation $\hat{V}$ includes two terms, the geometric inductance and the Josephson one:

$$\hat{V} = \underbrace{-\frac{E_J\phi^4}{24}}_{\substack{\text{nonlinear}\\ \text{part of JJ}}} \underbrace{-\frac{E_J}{2}\left(\frac{1}{\gamma} - 1\right)\frac{\phi^4}{3}}_{\substack{\text{nonlinear part}\\ \text{due to}\\ \Phi^2_{\text{geom}} \sim \sin^2\phi}}. \tag{4}$$

Following the Landau-Lifshitz approach for the shifting levels of a harmonic oscillator [48], we can write

$$\hat{V} = \beta\Phi^4, \tag{5}$$

where

$$\beta = \left[-\frac{E_J}{24} - \frac{E_J}{6}\left(\frac{1}{\gamma} - 1\right)\right]\frac{\gamma^2}{L^2E_J^2}. \tag{6}$$

The shift of the energy levels is

$$\Delta E_n = \frac{3}{2}\beta\left(\frac{\hbar}{m\omega}\right)^2\left(n^2 + n + \frac{1}{2}\right), \tag{7}$$

where n is the number of energy levels and $\hbar$ is Planck's constant. Thus, the anharmonicity of the meta-atom is

$$\begin{aligned}\alpha &\equiv (E_1^* - E_0^*) - (E_2^* - E_1^*)\\ &= 2\Delta E_1 - \Delta E_0 - \Delta E_2 = -3\beta\left(\frac{\hbar}{m\omega}\right)^2,\end{aligned} \tag{8}$$

where m is the generalized mass,

$$m = C = \frac{1}{\omega^2 L} \rightarrow \frac{\hbar}{m\omega} = hfL, \tag{9}$$

with $h = 2\pi\hbar$ and $\omega = 2\pi f$. Substituting β from Eq. (6) into Eq. (8), we can describe the anharmonicity α of the meta-atom using the γ parameter:

$$\alpha = \frac{(hf)^2}{E_J}\left(\frac{\gamma^2}{8} + \frac{\gamma - \gamma^2}{2}\right). \tag{10}$$

We use Eq. (10) to calculate the anharmonicity in the simulation. If $\gamma = 1$, Eq. (10) represents the transmon anharmonicity [49].

It follows from Eq. (10) that the meta-atom must provide strong concentrated magnetic fields at the JJ origin to achieve a high value of the anharmonicity α. Moreover, the role of dielectric losses in JJs was recently marked as a potentially crucial channel of relaxation in superconducting qubits due to the interaction with electric fields [49]. Thus, we conclude that W^E should be lower close to the JJ. In this case, we expect a significant anharmonicity of the meta-atom, provided that $W_H \gg W_E$ close to the JJ.

For this aim, we propose a superconducting anapole meta-atom designed as a hybrid split ring resembling the symbol $\in$, which has voids embedded in a superconductor layer, as depicted in Fig. 1(a). By the excitation of the meta-atom by the external wave with electric field $\boldsymbol{E}$ parallel to the central wire, this configuration supports two circular current loops $\boldsymbol{j}$ along the edges. Each current induces the circulating magnetic field (moments $\boldsymbol{m}$) writhing around the central part of the metamolecule. As a result, this leads to a toroidal moment $\boldsymbol{T}$ oscillating back and forth along the axis of the meta-atom. Moreover, due to the central wire, the electric dipole moment $\boldsymbol{P}$ can be excited in the system [Fig. 1(a)].

Our goal is strong localization of the magnetic field in the region of the central wire of the meta-atom, where the JJ element is placed. Such a configuration of the fields will ensure high anharmonicity of the system, according to Eq. (10). Accordingly, we expect the excitation of the anapole state in the meta-atom, which suppresses radiating losses, leading to the localization of a strong magnetic field [50,51].

For excitation of the meta-atom, we exploit the TM_{01} circular waveguide mode, as shown in Figs. 1(b) and 1(c). We design a metallic waveguide with dimensions D and L_a

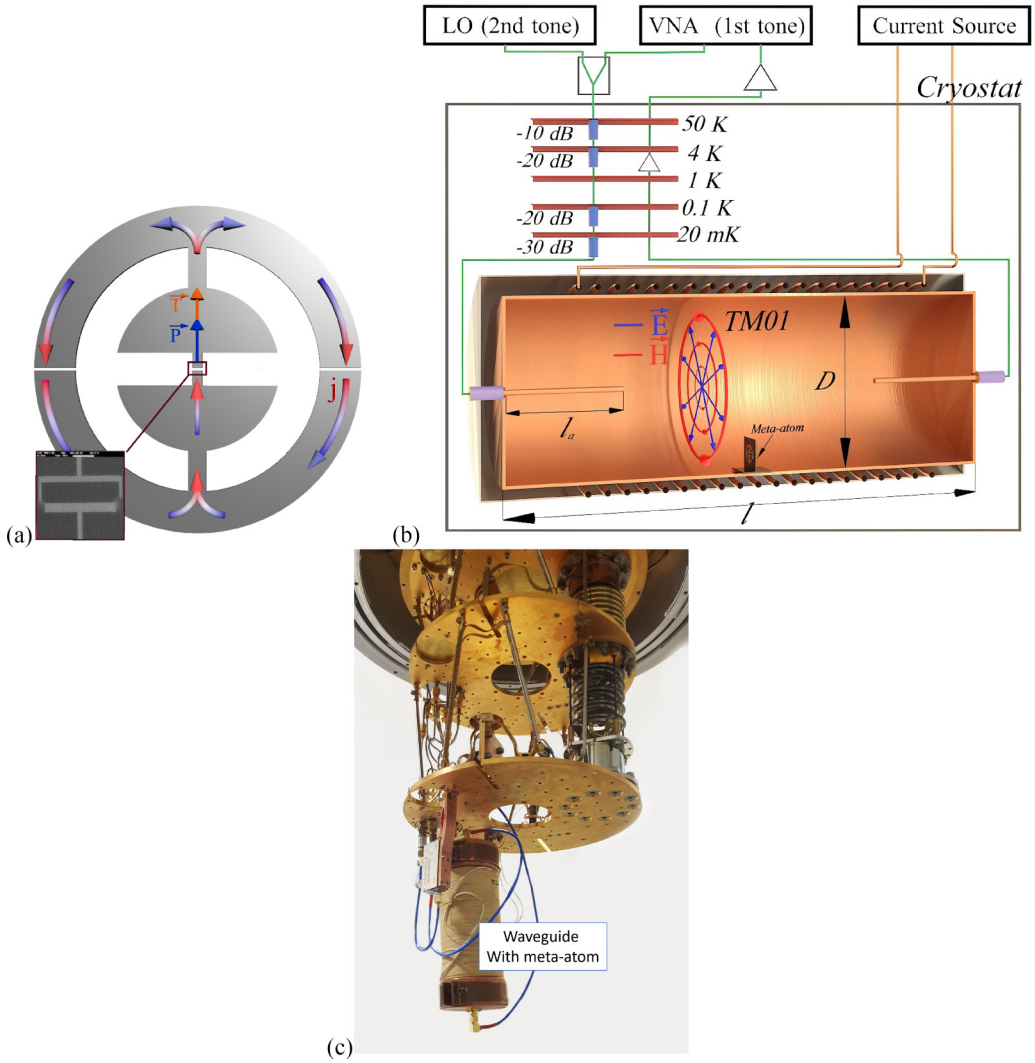

FIG. 1. (a) The scheme of an anapole meta-atom with an embedded SQUID and poloidal current distributions **j** induced by waveguide mode TM01. (b) Experimental setup of single-tone and two-tone spectroscopy. The waveguide with the meta-atom is placed in a cryostat on a 20 mK plate. Each of the attenuators (from −10 to −30 dB attenuation) is included at each stage to suppress thermal noise that propagates further down the system. A signal generator, a vector network analyzer, and a current source are used to control the system. (c) Photo of the experimental setup with a waveguide in the cryostat.

(see Table I) in order to have the frequency regime of the meta-atom close to the cutoff frequency $f_{\text{cut}} = 4.2$ GHz.

TABLE I. Dimensions of the structure.

Resonator		SQUID	
Parameter	Value	Parameter	Value
R_{in} (mm)	1.5	J_c (μA/μm^2)	1.92
R_{middle} (mm)	2.3	C_s (fF)	10
R_{out} (mm)	3	S_1 (nm^2)	150 × 167
g (mm)	0.05	S_2 (nm^2)	150 × 267
s (mm)	0.6	L_{max} (nH)	11.3
b (mm)	0.3	L_{min} (nH)	2.63
D (mm)	56.5		
L (mm)	160		

Indeed, the scattering from a meta-atom placed in a waveguide should be suppressed for frequencies close to the cutoff regime. This suppression is similar to the effect of a radiating atom located in the band gap or near it, leading to the enhancement of the Q factor of a resonator tuned below the cutoff frequency [52]. Due to the weak coupling of the meta-atom with the waveguide, the width of the spectral lines should be narrowed. If several spectral lines are required to observe the desired quantum effect, then this procedure becomes more promising. The TM_{01} mode of the waveguide has the configuration presented in Fig. 1(b), with electric field lines distributed radially and magnetic fields circulating in the cross section of the waveguide.

For the simulation of electromagnetic properties of meta-atoms, we use a commercial version of the COMSOL MULTIPHYSICS software based on the numerical calculation of Maxwell's equations. For simulation of JJs, we use a lumped element with an inductance of 2.6 nH, which corresponds to

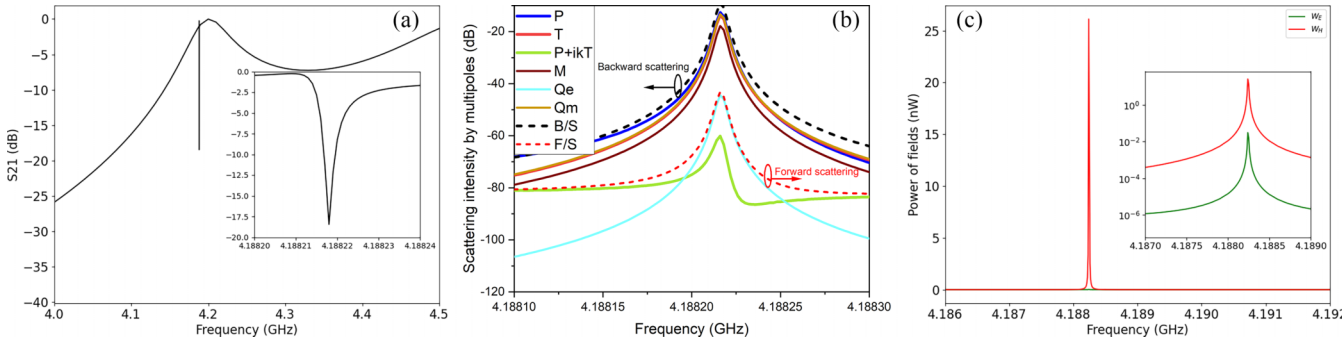

FIG. 2. (a) Transmission spectrum S_{21} waveguide system with a meta-atom. (b) Intensity of the radiated multipoles excited in the meta-atom. F/S = forward scattering; B/S = backward scattering. (c) The energies of the electric field W_E and the magnetic field W_H integrated over the entire volume around the central area with the JJ. The inset is shown on a logarithmic scale.

$E_j = 63.1$ GHz. The meta-atom and waveguide are assumed to be a perfect electric conductor. The meta-atom is excited by the coaxial connector on the front wall of the circular waveguide The second connector (for receiving the signal from the meta-atom) was placed on the back wall of the waveguide [Fig. 1(b)]. We simulate the parameters of the transmission spectrum S_{21} of the waveguide with the meta-atom [Fig. 2(a)], as well as the distribution of electric [Fig. 3(a)] and magnetic [Fig. 3(b)] fields and induced currents [Fig. 3(c)] in the meta-atom. The S_{21} parameter refers to the transmission coefficient, specifically to the ratio of the power transmitted from the input port of the waveguide to the power received at the output port. The presence of axial adapters for the feed of the waveguide leads to the fact that the actual cutoff frequency of the waveguide is higher than that for an infinite waveguide with the same diameter. The feed diameters are the same, 1.3 mm.

We perform a simulation of the S_{21} parameters of the waveguide with a meta-atom in the microwave frequency range of 3.9–4.5 GHz [Fig. 2(a)]. At the frequency 4.418822 GHz, we observe a narrow resonance spectral line with a very high Q factor, 1.4×10^6.

Besides the fact that the anapole character of our design can be confirmed by extremely narrow resonance, there is the distribution of the near fields and the density of the displacement currents induced in the meta-atom (Fig. 3). The magnetic field at the resonance frequency corresponds to the closed vortex localized close to the central wire with the JJ of the meta-atom. At the same time, the electric field is localized beyond the JJ and distributed in the periphery of the meta-atom. Moreover, the current density resembles the two closed loops of poloidal currents in the cross section of the torus. These two loops generate a magnetic vortex with strong intensity around the JJ. Such current and field distributions confirm the anapole manifestation at the resonance frequency, 4.18822 GHz.

To assess the role of the multipole contribution in forming the observed response, we calculate the intensities of the multipoles in terms of the electromagnetic power they scatter in the far-field zone [see Appendix A, Eq. (A1)]. These contributions of the multipole moments induced in the meta-atom by the waveguide mode are calculated on the basis of the density of the conducting currents excited in the meta-atom [Fig. 2(b)]. The resonance is defined by the contribution of the electric ($\boldsymbol{P}$) and toroidal dipole ($\boldsymbol{T}$) moments and the suppressed electric quadrupole Q_e. In the narrow frequency range close to 4.418 GHz, the power radiated by the toroidal dipole moment $\boldsymbol{T}$ prevails in the system and is equal to the power of the electric dipole moment $\boldsymbol{P}$. This corresponds to the dynamic anapole excitation in the meta-atom, where far-field scattering of the electric type is sufficiently suppressed due to the destructive interference term ($\boldsymbol{P} + ik\boldsymbol{T}$) between the toroidal and electric dipole excitations. As a result, the intensity of the interference term is lower than that of the magnetic-type multipoles (the magnetic dipole moment and quadrupole). Due to such decomposition of the multipoles, the response of the meta-atom represents the suppressed electric radiation due to the anapole state and magnetic type due to the excited magnetic dipole and magnetic quadrupole in the system [50,51]. At the same time, this corresponds to suppressed electric near fields, while magnetic fields are

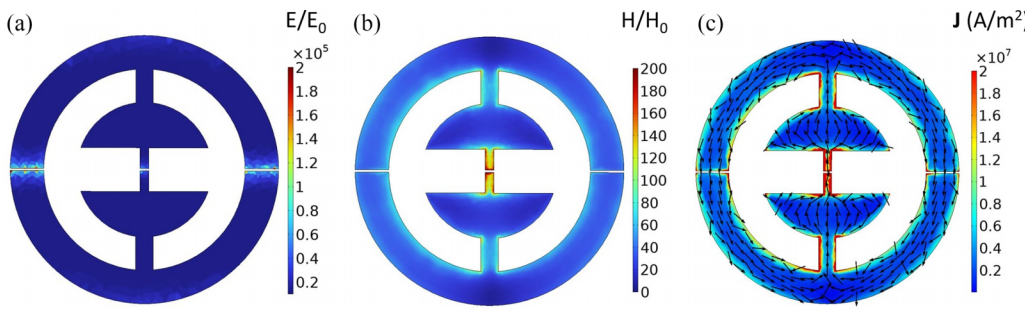

FIG. 3. The distibutions of (a) The electric and (b) magnetic fields and (c) current density at a resonance frequency of 4.18822 GHz in meta-atom.

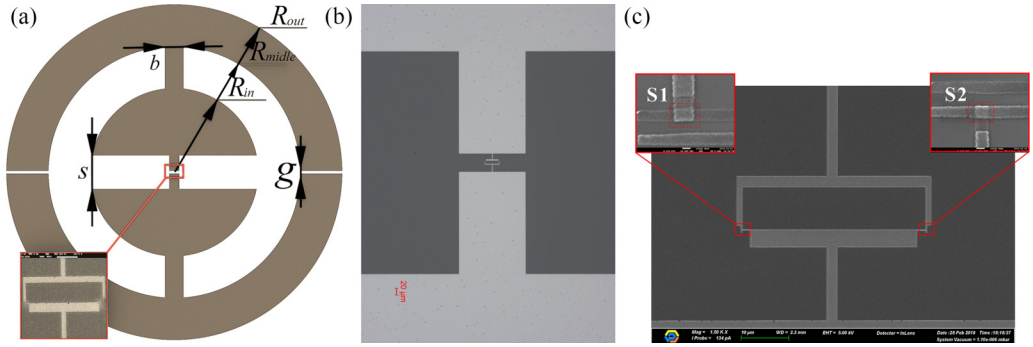

FIG. 4. (a) The scheme of an anapole meta-atom with an embedded SQUID and parameters presented in Table I. (b) Fragment of a scanning electron microscope (SEM) image of the meta-atom with an embedded SQUID. (c) SEM image of SQUID elements S1 and S2.

enhanced in the area around the JJ. Moreover, we add to Fig. 2(b) the total scattering intensity in the forward scattering and backward scattering directions. The total scattering intensities in the forward and backward directions are restored from a sum of scattered multipoles in those directions. We note that the intensity in the forward direction is very low, less than -50 dB, and is defined by the dynamic anapole ($\boldsymbol{P} + ik\boldsymbol{T}$), which suppresses forward radiation up to a very low electric quadrupole intensity. At the same time, the intensity in the backward direction is defined by magnetic quadrupole radiation accompanying all toroidal-like structures [36]. This parasitic contribution of the magnetic quadrupole is a general limitation of the high Q factor of anapole metaparticles.

We also plot the energy of the electric and magnetic fields around the JJ, where the superconducting quantum interference device (SQUID) is placed, in Fig. 2(c). The integration region is determined by the distance from the JJ at which the magnetic field drops to zero, i.e., 500 μm. The enhancement of the magnetic field energy W_H close to the resonance frequency of 4.418822 GHz is more than 10^3 times that of the electric field energy W_E. At the same time, the calculated value of γ is 9×10^{-2}. For comparison, $\gamma = 10^{-7}$ for an empty waveguide with an area without a JJ. Thus, the strong localization of the magnetic field in the JJ region is obvious for an anapole meta-atom. According to Eq. (10), the anharmonicity of the meta-atom is $\alpha = 0.5$ MHz.

III. SAMPLE FABRICATION

For experimental observation of the meta-atom anharmonicity, we fabricate a two-terminal asymmetric SQUID with different areas of Josephson contacts S_1 and S_2 for the possibility of adjusting the frequency of a meta-atom and unambiguously identifying it in the spectra (Fig. 4).

We fabricated the SQUID by sputtering aluminum on a Si substrate film. Oxidation occurred in an atmosphere of pure oxygen with a partial pressure of 0.01–2 mbar, which is admitted into a vacuum chamber. The peculiarity of this oxidation is that oxygen ceases to diffuse into aluminum at a very small thickness of the amorphous oxide film (on the order of 2–3 nm), which is excellent for the formation of a Josephson bond with critical current densities of the order of 0.1–10 μA/μm^2. As a result, an $\mathrm{Al} - \mathrm{AlO}_x\text{-Al}$ Josephson junction is fabricated at the same aluminum is widely used as a superconducting metal.

The sample was fabricated on a high-resistivity Si wafer (10 kΩ cm, 500 μm thick) prepared by piranha-based wet cleaning and a HF dip to remove surface oxide damage. First, a two-layer electron-beam resist stack (MMA/PMMA) is spin coated, followed by 50 kV electron-beam exposure [53]. After development and oxygen plasma treatment, we performed UHV electron-beam shadow evaporation of the $\mathrm{Al} - \mathrm{AlO}_x\text{-Al}$ SQUID ($\pm 11^\circ$) with oxidation in pure oxygen [54]. Finally, *N*-methyl-2-pyrrolidone at 80 °C followed by IPA was used to lift off the resist mask. The frequency of the meta-atom is controlled by an external magnetic field created by an inductance coil connected to a current source.

IV. EXPERIMENT

The waveguide with the meta-atom is placed on the bottom plate of a Bluefors LD250 cryostat at a temperature of 20 mK. Each level of the cryostat is equipped with *attenuators* to reduce thermal noise with different attenuation values, from 10 to 30 dB. The output signal has very low intensity. To compensate for losses before the first amplification, the output coaxial lines are made superconductive from the waveguide to the low-temperature amplifier at 4 K [Figs. 1(b) and 1(c)].

For the experimental study of the meta-atom response, we perform single-tone [Fig. 5(a)] and two-tone [Fig. 5(b)] spectroscopy [55] in a dilution cryostat and control the electronics at room temperature.

A. Single-tone spectroscopy

In the case of single-tone spectroscopy, we measure the dispersion of the S_{21} parameters (transmission) using an Agilent N5242A vector network analyzer [Fig. 5(a)]. The resonance close to 4 GHz has Fano-like shape and is described by the Fano formula, which is consistent with a Lorentzian, if $q \to \pm\infty$ or $q = 0$: $I(\omega) = \frac{1}{q^2+1}\frac{[q+(\omega-\omega_0)/\Gamma]^2}{1+[(\omega-\omega_0)/\Gamma]^2}e^{-2\pi\imath f\tau}$, where q is the Fano parameter, ω_0 is the resonance frequency, Γ is the resonance width, and $e^{-2\pi\imath f\tau}$ is the signal delay [56]. In the ranges $-\infty < q < 0$ and $0 < q < +\infty$, the spectrum corresponds to a narrow asymmetric line. We approximate the S_{21} parameter obtained in an experiment with the Fano formula with parameters $q = 4.61$ and $g = 320$ kHz and calculate the Q factor of the resonance: $Q = 11564$. In the next step, we perform single-tone spectroscopy of the meta-atom and observe the dependence of S_{21} on the external magnetic

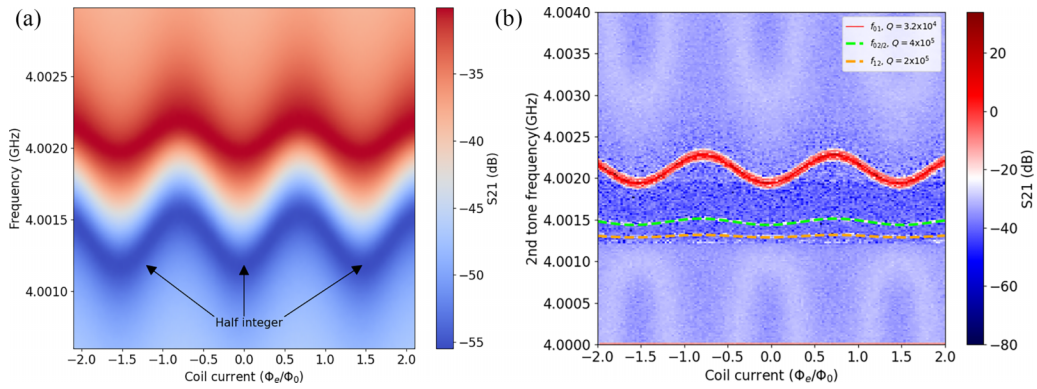

FIG. 5. (a) The results of single-tone spectroscopy performed at a signal power on a vector network analyzer of −20 dBm (0.01 mW). (b) The results of two-tone spectroscopy at −60 dBm signal power on a vector network analyzer and with the resonant frequency pumped by a generator with a power of 14 dBm.

flux (flux dispersion). The results are presented in Fig. 3(a). If a half-integer number of flux quanta are excited in the SQUID loop, then the critical current is minimal, which corresponds to the maximum inductance, and the frequency is minimal here. The critical current of the SQUID is in the range of 29–125 nA, which corresponds to inductance values from 2.6 to 11.4 nH. The Josephson energy in this case varies in the range from 14 to 62 GHz. We control the critical current on the SQUID by tuning the external magnetic flux penetrating the waveguide along its longitudinal axis. We fabricate the waveguide from copper so that the magnetic field has the possibility of penetrating through the waveguide walls. The current in the coil encircling the waveguide changes with a step of 0.028 mA. This gives us the possibility to find the meta-atom resonance frequency at various flux values and, in particular, to define the optimal points in the spectra for pumping a meta-atom with two-tone spectroscopy. We find a resonance flux dispersion close to 4.001 GHz in the spectra.

B. Two-tone spectroscopy

To observe the anharmonicity of the meta-atom, we measure its different quantum levels using two-tone spectroscopy [Fig. 5(b)]. For this aim, we excite the input of the waveguide using two signals. The vector network analyzer still operates as the first tone, providing a dispersive measurement of the S_{21} parameters. The second tone signal of an Agilent E8257D analog signal generator *local oscillator* (LO) pumps the meta-atom in the scanning frequency regime. Since the signals at different frequencies almost do not interfere, both signals can be fed through one channel by combining them through a *splitter* [black rectangle in Fig. 1(b)]. If the current in the coil changes, the resonance frequency changes according to a sinusoidal law; therefore, in order to remain at the peak position of the resonance, the frequency of the LO is automatically adjusted according to a previously performed calibration using single-tone spectroscopy.

The resonance has flux dispersion and is presented as an eigenmode of the meta-atom in the linear approximation together with a nonlinear element, the SQUID. If the number of flux quanta in the SQUID is an integer or half integer, $\frac{\partial f}{\partial \Phi_{\text{ext}}} = 0$, in the vicinity of the corresponding current values through the solenoid, the SQUID has the most stable inductance, including stable nonlinear parameters.

The result of the two-tone spectroscopy is presented as a map of transmission coefficients S_{21} in the frequency range close to 4.001 GHz in Fig. 5(b). Applying the second tone allows the meta-atom to be pumped at the ground anapole state frequency, leading to the degeneracy of higher energy excited levels. The first tone makes it possible to observe this degeneration; on the spectrum of two-tone spectroscopy, one can see a series of curves corresponding to transitions [Fig. 5(b)] $|1\rangle \rightarrow |2\rangle$ and $|0\rangle \rightarrow |2\rangle$. In the two-tone spectroscopy spectrum, several single-photon transitions can be observed, $|0\rangle \rightarrow |1\rangle$ ($f_{01} = 4.0021$ GHz) and $|1\rangle \rightarrow |2\rangle$ ($f_{12} = 4.0013$ GHz), as well as the two-photon transition $|0\rangle \rightarrow |2\rangle$ ($f_{02}/2 = 4.0015$ GHz). To identify transition levels, we use the approach of Probst *et al.* for the approximation of two-tone spectroscopy [56]. This approach allows one to calculate the resonance frequency of f_r of the linear system $f_{\text{lin}} = 4.0020$ GHz. The energy levels of the excited meta-atom are expressed as

$$E_n^*/h = (f_{\text{lin}} + 1/2) - \alpha/2(n^2 + n + 1/2), \tag{11}$$

where the left term describes the energy levels of the harmonic (unperturbed) system E_n and the right term corresponds to the disturbance $\Delta E_n = E_n^* - E_n$, with anharmonicity $\alpha = f_{01} - f_{12}$. Then we can write expressions for the frequencies of the transition levels [56]:

$$f_{01} = E_1^* - E_0^* = f_{\text{lin}} - \alpha, \tag{12}$$

$$f_{12} = E_2^* - E_1^* = f_{\text{lin}} - 2\alpha, \tag{13}$$

$$f_{02/2} = (E_2^* - E_0^*)/2 = f_{\text{lin}} - 3/2\alpha. \tag{14}$$

The red curve in Fig. 5(b) shows the main state of the meta-atom, $f_{01} = 4.0021$ GHz, to which the adjustable second tone is tuned. Two additional peaks can be seen on the spectrum, corresponding to the transition level $f_{12} = 4.0013$ GHz and the two-photon transition level $f_{02}/2 = 4.0015$ GHz. The experimental anharmonicity on the spectrum is found to be $\alpha = 540$ kHz, which is in good agreement with the value $\alpha = 500$ kHz obtained in the simulations using Eq. (10).

V. DISCUSSION

In this paper, we aim to demonstrate a proof-of-concept experiment for various quantum applications of giant anapole meta-atoms in the context of quantum elements of two-level systems, sensors, and lasers and, especially, for quantum computing. The advantage is the suppressed radiating losses and, consequently, a colossal Q factor. Moreover, the use of the nonradiating anapole state gives us possibilities for resolving the few transition levels of the meta-atom with a giant superconducting surface area of 20 mm^2, which is an order of magnitude larger than that in standard qubit designs, despite the measured anharmonicity of the meta-atom of 0.54 MHz. Moreover, the advantage of large-scale anapole superconducting systems is their susceptibility to local thermal overheating. The suppression of both radiating and dissipative losses can increase the coherence time, which allows us to represent proposed meta-atoms as qubits. The most essential characteristics of quantum meta-atoms are the times of radiative and nonradiative relaxation. Here, we perform the fitting of single-tone spectra according to the asymmetric Lorentz formula [56]. However, for real devices, the model becomes more complicated: $S_{21}(f) = A_0 e^{i\psi} e^{2\pi i f \tau}[1 - \frac{Q_l/|Q_c|}{1+2iQ_l(f/f_m-1)}]$. This equation includes the attenuation (amplification) of the signal A_0; the frequency-dependent phase shift ψ; the delay τ, which occurs due to the delay in signal propagation through the system; and the frequency of the meta-atom f_m. The coupling of the anapole meta-atom to the waveguide is characterized by the complex Q factor $Q_c = 3249$ [57], which describes the radiative relaxation rate $\Gamma_1^r/2\pi = f_q/Q_c = 1.23$ MHz. The loaded Q factor of the waveguide with the meta-atom ($Q_l = 11\,564$) describes the internal losses of the system, demonstrating all kinds of reasons why the coherent signal does not properly reach the vector network analyzer after scattering by the meta-atom [$1/Q_i = 1/Q_l - 1/\mathrm{Re}(Q_c) = 1/4518$]. The nonradiative relaxation includes losses in the meta-atom and relaxation of any parasitic modes of the waveguides, as well as dephasing: $(\Gamma_1^{nr} + 2\Gamma_\phi)/2\pi = f_q/Q_i = 0.9$ MHz. For advanced qubit applications the coherence time should be longer than the duration of the control pulses (4–20 ns) [58]. The proposed meta-atom operates in the $\Gamma_2 \approx \Gamma_1$ regime due to a sufficiently high nonradiative relaxation. However, the obtained rates of radiative and nonradiative relaxation are comparable to those of the well-known transmon and fluxonium qubits [59,60], indicating that our system has sufficiently large dimensions and can find applications as a large-scale *anapole qubit* compared with the wavelength.

VI. CONCLUSION

In this paper, we proposed a model of a quantum meta-atom with an anapole response. Due to nonradiating properties of the anapole state and strong field localization, we demonstrated the anharmonicity of a superconducting Al meta-atom with an embedded Josephson junction. We performed microwave single- and two-tone spectroscopy of the meta-atom in the waveguide within a dilution cryostat at 20 mK and demonstrated three transition energy levels: single-photon and two-photon transitions. The experimental anharmonicity is 540 kHz, which is very close to the value of 500 kHz obtained in simulations. Our anapole approach could be promising for giant qubits for quantum computing.

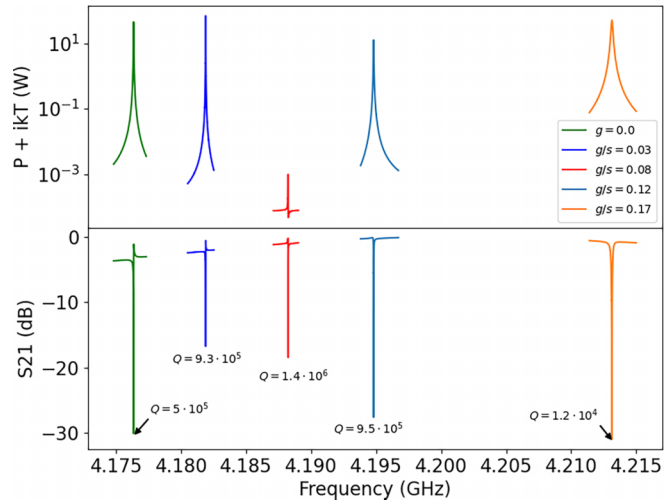

FIG. 6. Optimization of the g parameter in the range of 0–0.1 mm, where 0 mm means that the meta-atom is formed by a closed ring; this option excludes the possibility of using the SQUID restructuring due to the Meissner effect. The operating mode is shown by the red line. The anapole state is the effect of radiation suppression in the far-field zone, with a maximum loaded quality factor $Q = 1.4 \times 10^6$.

ACKNOWLEDGMENTS

We acknowledge support from the Ministry of Education and Science of the Russian Federation in the framework of the Program of Strategic Academic Leadership "Priority 2030" (Strategic Project "Quantum Internet"). The theoretical part of this work was supported by the Russian Foundation for Basic Research, Project No. 20-32-90153. The samples were fabricated at the BMSTU Nanofabrication Facility (Functional Micro/Nanosystems, FMNS REC, ID 74300)

APPENDIX A: MULTIPOLE DECOMPOSITION

We use a multipole decomposition approach to correctly determine the radiating properties of the meta-atom. In the multipole decomposition presentation, the power of the radiating multipoles can be written as [40]

$$P_{\mathrm{sca}} \simeq \frac{k_0^4\sqrt{\varepsilon_s}}{12\pi\varepsilon_0^2 c\mu_0}\left|\mathbf{P} + \frac{ik_0}{c}\varepsilon_s\mathbf{T}\right|^2 + \frac{k_0^4\varepsilon_s\sqrt{\varepsilon_s}}{12\pi\varepsilon_0 c}|\mathbf{M}|^2 + \frac{k_0^6\varepsilon_s\sqrt{\varepsilon_s}}{160\pi\varepsilon_0^2 c\mu_0}\sum_{\alpha\beta}|Q_{e,\alpha\beta}| + \frac{k_0^6\varepsilon_s^2\mu_0}{80\pi\varepsilon_0}\sum_{\alpha\beta}|Q_{M,\alpha\beta}|^2, \tag{A1}$$

where c is the speed of light in vacuum, $\mathbf{P}$, $\mathbf{T}$, $\mathbf{M}$, $\hat{Q}_e$, and $\hat{Q}_m$ are the electric dipole, toroidal dipole, magnetic dipole, electric quadrupole, and magnetic quadrupole moments, respectively. Explicit definitions of the multipoles in Eq. (A1) are listed in Table II. Using Eq. (A1), one can analyze the individual contributions of various multipole terms to the power radiated by multipoles. In this paper, we use the definitions of the electric quadrupole tensors $\hat{Q}_e$ and $\hat{T}^Q$ (see Table II). To

TABLE II. Multipole moments determining the power radiated by multipoles, which are expressed by Eq. (A1). The multipole moments are calculated with respect to the origin of the Cartesian coordinate system. V is the total volume of the meta-atom in the system, and ω is the angular frequency of the incident wave [the time dependence $\exp(-i\omega t)$ is assumed]. ED, electric dipole; TD, toroidal dipole; MD, magnetic dipole; EQ, electric quadrupole; MQ, magnetic quadrupole.

ED: $\mathbf{P} = \frac{i}{\omega}\int_V \mathbf{j}\, d\mathbf{r}$	TD: $\mathbf{T} = \frac{1}{10}\int_V [(\mathbf{r}\cdot\mathbf{j})\mathbf{r} - 2r^2\mathbf{j}]d\mathbf{r}$
MD: $\mathbf{M} = \frac{1}{2}\int_V [\mathbf{r}\times\mathbf{j}]d\mathbf{r}$	
MQ: $\hat{Q}_m = \frac{1}{3}\int_V ([\mathbf{r}\times\mathbf{j}]\otimes \mathbf{r} + \mathbf{r}\otimes[\mathbf{r}\times\mathbf{j}])d\mathbf{r}$	
EQ: $\hat{Q}_e = \frac{3i}{\omega}\int_V (\mathbf{j}\otimes\mathbf{r} + \mathbf{r}\otimes\mathbf{j} - \frac{2}{3}(\mathbf{r}\cdot\mathbf{j})\hat{U})d\mathbf{r}$	

calculate the multipole contributions (Table II), using (A1), we integrate the current densities excited in the meta-atom by the waveguide mode obtained with simulations using COMSOL MULTIPHYSICS for frequencies close to resonance. We take into account the fact that the radiation centers of the multipoles coincide with the geometrical center of the meta-atom [61–64].

APPENDIX B: SIMULATION

In order to optimize the anapole meta-atom design, we study the meta-atom response for various values of lateral gaps. Figure 6 shows the results of our simulations for gaps varying in the range of 0–0.1 μm. From the graph of the interference term intensity between the electric and toroidal multipoles it follows that for a gap $g = 0.05$ μm, the Q factor is maximum, indicating that the electric and toroidal multipoles exist in an anapole state. However, for other gaps, the interference terms of the multipoles are higher, and the Q factor is 10 times less than that for $g = 0.05$ μm.

[1] J. P. Dowling and G. J. Milburn, Quantum technology: The second quantum revolution, Philos. Trans R. Soc. London, Ser. A **361**, 1655 (2003).

[2] D. J. Griffiths and D. F. Schroeter, *Introduction to Quantum Mechanics* (Cambridge University Press, Cambridge, 2018).

[3] R. P. Feynman, R. B. Leighton, and M. Sands, *The Feynman Lectures on Physics, Vol. III: Quantum Mechanics* (Addison-Wesley, 1965).

[4] A. Zagoskin, *Quantum Mechanics: A Complete Introduction: Teach Yourself* (Hodder, Hachette, UK, 2015).

[5] I. Buluta, S. Ashhab, and F. Nori, Natural and artificial atoms for quantum computation, Rep. Prog. Phys. **74**, 104401 (2011).

[6] R. Blatt and D. Wineland, Entangled states of trapped atomic ions, Nature (London) **453**, 1008 (2008).

[7] W. Unrau and D. Bimberg, Flying qubits and entangled photons, Laser Photonics Rev. **8**, 276 (2014).

[8] M. Kjaergaard, M. E. Schwartz, J. Braumüller, P. Krantz, J. I.-J. Wang, S. Gustavsson, and W. D. Oliver, Superconducting qubits: Current state of play, Annu. Rev. Condens. Matter Phys. **11**, 369 (2020).

[9] M. H. Devoret and R. J. Schoelkopf, Superconducting circuits for quantum information: An outlook, Science **339**, 1169 (2013).

[10] A. A. Houck, J. Koch, M. H. Devoret, S. M. Girvin, and R. J. Schoelkopf, Life after charge noise: Recent results with transmon qubits, Quantum Inf. Process. **8**, 105 (2009).

[11] C. Wang, X. Li, H. Xu, Z. Li, J. Wang, Z. Yang, Z. Mi, X. Liang, T. Su, C. Yang *et al.*, Towards practical quantum computers: Transmon qubit with a lifetime approaching 0.5 milliseconds, npj Quantum Inf. **8**, 3 (2022).

[12] A. Somoroff, Q. Ficheux, R. A. Mencia, H. Xiong, R. Kuzmin, and V. E. Manucharyan, Millisecond coherence in a superconducting qubit, Phys. Rev. Lett. **130**, 267001 (2023).

[13] L. B. Nguyen, Y.-H. Lin, A. Somoroff, R. Mencia, N. Grabon, and V. E. Manucharyan, High-coherence fluxonium qubit, Phys. Rev. X **9**, 041041 (2019).

[14] I. Moskalenko, I. Besedin, I. Simakov, and A. Ustinov, Tunable coupling scheme for implementing two-qubit gates on fluxonium qubits, Appl. Phys. Lett. **119**, 194001 (2021).

[15] I. Siddiqi, Engineering high-coherence superconducting qubits, Nat. Rev. Mater. **6**, 875 (2021).

[16] B. Kannan, M. J. Ruckriegel, D. L. Campbell, A. Frisk Kockum, J. Braumüller, D. K. Kim, M. Kjaergaard, P. Krantz, A. Melville, B. M. Niedzielski *et al.*, Waveguide quantum electrodynamics with superconducting artificial giant atoms, Nature (London) **583**, 775 (2020).

[17] A. Krasnok, P. Dhakal, A. Fedorov, P. Frigola, M. Kelly, and S. Kutsaev, Superconducting microwave cavities and qubits for quantum information systems featured, Appl. Phys. Rev. **11**, 011302 (2024).

[18] A. M. Zagoskin, A. Chipouline, E. Il'ichev, J. R. Johansson, and F. Nori, Toroidal qubits: Naturally-decoupled quiet artificial atoms, Sci. Rep. **5**, 16934 (2015).

[19] A. E. Miroshnichenko, A. B. Evlyukhin, Y. F. Yu, R. M. Bakker, A. Chipouline, A. I. Kuznetsov, B. Luk'yanchuk, B. N. Chichkov, and Y. S. Kivshar, Nonradiating anapole modes in dielectric nanoparticles, Nat. Commun. **6**, 8069 (2015).

[20] V. A. Fedotov, A. Rogacheva, V. Savinov, D. P. Tsai, and N. I. Zheludev, Resonant transparency and non-trivial non-radiating excitations in toroidal metamaterials, Sci. Rep. **3**, 2967 (2013).

[21] R. M. Saadabad, L. Huang, A. B. Evlyukhin, and A. E. Miroshnichenko, Multifaceted anapole: From physics to applications, Opt. Mater. Express **12**, 1817 (2022).

[22] K. V. Baryshnikova, D. A. Smirnova, B. S. Luk'yanchuk, and Y. S. Kivshar, Optical anapoles: Concepts and applications, Adv. Opt. Mater. **7**, 1801350 (2019).

[23] V. Savinov, N. Papasimakis, D. Tsai, and N. Zheludev, Optical anapoles, Commun. Phys. **2**, 69 (2019).

[24] M. V. Cojocari, A. K. Ospanova, V. I. Chichkov, M. Navarro-Cia, A. Gorodetsky, and A. A. Basharin, Pseudo-anapole regime in terahertz metasurfaces, Phys. Rev. B **104**, 075408 (2021).

[25] A. C. Tasolamprou, O. Tsilipakos, A. Basharin, M. Kafesaki, C. M. Soukoulis, and E. N. Economou, Toroidal multipoles in metamaterials, in *Compendium on Electromagnetic Analysis: From Electrostatics to Photonics: Fundamentals and*

Applications for Physicists and Engineers, *Optics and Photonics II* (World Scientific, Singapore, 2020), Vol. 5, pp. 237–278.

[26] Y. Yang, V. A. Zenin, and S. I. Bozhevolnyi, Anapole-assisted strong field enhancement in individual all-dielectric nanostructures, ACS Photonics **5**, 1960 (2018).

[27] E. Takou, A. C. Tasolamprou, O. Tsilipakos, Z. Viskadourakis, M. Kafesaki, G. Kenanakis, and E. N. Economou, Anapole tolerance to dissipation losses in thermally tunable water-based metasurfaces, Phys. Rev. Appl. **15**, 014043 (2021).

[28] N. Pavlov, I. Stenishchev, A. Ospanova, P. Belov, P. Kapitanova, and A. Basharin, Toroidal dipole mode observation in situ, Phys. Status Solidi B **257**, 1900406 (2020).

[29] A. K. Ospanova, G. Labate, L. Matekovits, and A. A. Basharin, Multipolar passive cloaking by nonradiating anapole excitation, Sci. Rep. **8**, 12514 (2018).

[30] G. Labate, A. Alu, and L. Matekovits, Surface-admittance equivalence principle for nonradiating and cloaking problems, Phys. Rev. A **95**, 063841 (2017).

[31] A. A. Basharin, E. Zanganeh, A. K. Ospanova, P. Kapitanova, and A. B. Evlyukhin, Selective superinvisibility effect via compound anapole, Phys. Rev. B **107**, 155104 (2023).

[32] M. M. Bukharin, V. Y. Pecherkin, A. K. Ospanova, V. B. Il'in, L. M. Vasilyak, A. A. Basharin, and B. Luk'yanchuk, Transverse Kerker effect in all-dielectric spheroidal particles, Sci. Rep. **12**, 7997 (2022).

[33] G. Labate, A. K. Ospanova, N. A. Nemkov, A. A. Basharin, and L. Matekovits, Nonradiating anapole condition derived from Devaney-Wolf theorem and excited in a broken-symmetry dielectric particle, Opt. Express **28**, 10294 (2020).

[34] A. K. Ospanova, A. Karabchevsky, and A. A. Basharin, Metamaterial engineered transparency due to the nullifying of multipole moments, Opt. Lett. **43**, 503 (2018).

[35] N. A. Nemkov, A. A. Basharin, and V. A. Fedotov, Nonradiating sources, dynamic anapole, and Aharonov-Bohm effect, Phys. Rev. B **95**, 165134 (2017).

[36] A. A. Basharin, V. Chuguevsky, N. Volsky, M. Kafesaki, and E. N. Economou, Extremely high Q-factor metamaterials due to anapole excitation, Phys. Rev. B **95**, 035104 (2017).

[37] J. S. Totero Gongora, A. E. Miroshnichenko, Y. S. Kivshar, and A. Fratalocchi, Anapole nanolasers for mode-locking and ultrafast pulse generation, Nat. Commun. **8**, 15535 (2017).

[38] N. Papasimakis, V. Fedotov, V. Savinov, T. Raybould, and N. Zheludev, Electromagnetic toroidal excitations in matter and free space, Nat. Mater. **15**, 263 (2016).

[39] T. Kaelberer, V. Fedotov, N. Papasimakis, D. Tsai, and N. Zheludev, Toroidal dipolar response in a metamaterial, Science **330**, 1510 (2010).

[40] E. A. Gurvitz, K. S. Ladutenko, P. A. Dergachev, A. B. Evlyukhin, A. E. Miroshnichenko, and A. S. Shalin, The high-order toroidal moments and anapole states in all-dielectric photonics, Laser Photonics Rev. **13**, 1800266 (2019).

[41] M. Gupta and R. Singh, Toroidal metasurfaces in a 2D flatland, Rev. Phys. **5**, 100040 (2020).

[42] N. I. Zheludev and D. Wilkowski, The rise of toroidal electrodynamics and spectroscopy, ACS Photonics **10**, 556 (2023).

[43] I. Kuprov, D. Wilkowski, and N. Zheludev, Toroidal optical transitions in hydrogen-like atoms, Sci. Adv. **8**, eabq6751 (2022).

[44] I. B. Zel'Dovich, Electromagnetic interaction with parity violation, Sov. Phys. JETP **6**, 1184 (1958).

[45] N. A. Nemkov, I. V. Stenishchev, and A. A. Basharin, Nontrivial nonradiating all-dielectric anapole, Sci. Rep. **7**, 1064 (2017).

[46] E. Zanganeh, A. Evlyukhin, A. Miroshnichenko, M. Song, E. Nenasheva, and P. Kapitanova, Anapole meta-atoms: Nonradiating electric and magnetic sources, Phys. Rev. Lett. **127**, 096804 (2021).

[47] J. A. Schreier, A. A. Houck, J. Koch, D. I. Schuster, B. R. Johnson, J. M. Chow, J. M. Gambetta, J. Majer, L. Frunzio, M. H. Devoret, S. M. Girvin, and R. J. Schoelkopf, Suppressing charge noise decoherence in superconducting charge qubits, Phys. Rev. B **77**, 180502(R) (2008).

[48] L. D. Landau and E. M. Lifshitz, *Quantum Mechanics: Non-Relativistic Theory*, 3rd ed. (Pergamon Press, 1977).

[49] J. Koch, T. M. Yu, J. Gambetta, A. A. Houck, D. I. Schuster, J. Majer, A. Blais, M. H. Devoret, S. M. Girvin, and R. J. Schoelkopf, Charge-insensitive qubit design derived from the cooper pair box, Phys. Rev. A **76**, 042319 (2007).

[50] T. Feng, Y. Xu, W. Zhang, and A. E. Miroshnichenko, Ideal magnetic dipole scattering, Phys. Rev. Lett. **118**, 173901 (2017).

[51] B. Cappello, A. K. Ospanova, L. Matekovits, and A. A. Basharin, Mantle cloaking due to ideal magnetic dipole scattering, Sci. Rep. **10**, 2413 (2020).

[52] Y. Liu and A. A. Houck, Quantum electrodynamics near a photonic bandgap, Nat. Phys. **13**, 48 (2017).

[53] A. A. Pishchimova, N. S. Smirnov, D. A. Ezenkova, E. A. Krivko, E. V. Zikiy, D. O. Moskalev, A. I. Ivanov, N. D. Korshakov, and I. A. Rodionov, Improving Josephson junction reproducibility for superconducting quantum circuits: Junction area fluctuation, Sci. Rep. **13**, 6772 (2023).

[54] D. O. Moskalev, E. V. Zikiy, A. A. Pishchimova, D. A. Ezenkova, N. S. Smirnov, A. I. Ivanov, N. D. Korshakov, and I. A. Rodionov, Optimization of shadow evaporation and oxidation for reproducible quantum Josephson junction circuits, Sci. Rep. **13**, 4174 (2023).

[55] E. I. Kiselev, A. S. Averkin, M. V. Fistul, V. P. Koshelets, and A. V. Ustinov, Two-tone spectroscopy of a SQUID metamaterial in the nonlinear regime, Phys. Rev. Res. **1**, 033096(R) (2019).

[56] S. Probst, F. B. Song, P. A. Bushev, A. V. Ustinov, and M. Weides, Efficient and robust analysis of complex scattering data under noise in microwave resonators, Rev. Sci. Instrum. **86**, 024706 (2015).

[57] M. S. Khalil, M. J. A. Stoutimore, F. C. Wellstood, and K. D. Osborn, An analysis method for asymmetric resonator transmission applied to superconducting devices, J. Appl. Phys. **111**, 054510 (2012).

[58] T. D. Ladd, F. Jelezko, R. Laflamme, Y. Nakamura, C. Monroe, and J. L. O'Brien, Quantum computers, Nature (London) **464**, 45 (2010).

[59] A. Y. Dmitriev, R. Shaikhaidarov, T. Hönigl-Decrinis, S. E. de Graaf, V. N. Antonov, and O. V. Astafiev, Probing photon statistics of coherent states by continuous wave mixing on a two-level system, Phys. Rev. A **100**, 013808 (2019).

[60] A. N. Bolgar, J. I. Zotova, D. D. Kirichenko, I. S. Besedin, A. V. Semenov, R. S. Shaikhaidarov, and O. V. Astafiev, Quantum regime of a two-dimensional phonon cavity, Phys. Rev. Lett. **120**, 223603 (2018).

[61] R. E. Raab and O. L. De Lange, *Multipole Theory in Electromagnetism: Classical, Quantum, and Symmetry Aspects, with Applications* (Oxford University Press, Oxford, 2004), Vol. 128.

[62] V. R. Tuz, V. Dmitriev, and A. B. Evlyukhin, Antitoroidic and toroidic orders in all-dielectric metasurfaces for optical near-field manipulation, ACS Appl. Nano Mater. **3**, 11315 (2020).

[63] A. Ospanova, M. Cojocari, and A. Basharin, Modified multipoles in photonics, Phys. Rev. B **107**, 035156 (2023).

[64] A. Ospanova, M. Cojocari, P. Lamberti, A. Plyushch, L. Matekovits, Y. Svirko, P. Kuzhir, and A. Basharin, Broadband transparency of Babinet complementary metamaterials, Appl. Phys. Lett. **122**, 231702 (2023).